Proceedings of the Fifteenth International Conference on
Computational Structures Technology
Edited by: P. Iványi, J. Kruis and B.H.V. Topping
Civil-Comp Conferences, Volume 9, Paper 6.2
Civil-Comp Press, Edinburgh, United Kingdom, 2024
ISSN: 2753-3239, doi: 10.4203/ccc.9.6.2

Non-Material Finite Element Modelling of the Bending of a Rod, partially inserted in a Flexible Sleeve with Intrinsic Curvature

Y. Vetyukov

Institute of Mechanics and Mechatronics, TU Wien Vienna, Austria

Abstract

We consider frictionless contact between an elastic rod and a flexible sleeve. The rod is partially inserted into the sleeve, thus building a compound rod with piecewise constant bending stiffness and moving boundaries between the three segments: both the rod and the sleeve contribute to the bending stiffness in the overlapping segment. The intrinsic (natural) curvatures of the rod and the sleeve act as as load factors, resulting into bending, relative sliding and change of length of the segments. Concentrated contact interactions (configurational forces) at the transition points repel the rod and the sleeve from each other, eventually causing full ejection when the intrinsic curvatures exceed a threshold. To investigate this behavior, we apply a problem specific non-material finite element discretization of each segment of the elastic structure. Static equilibria are sought by augmenting the set of nodal degrees of freedom with the unknown configurational parameter, which determines sliding motion. After demonstrating the mesh convergence of the computational model, we investigate the parameter space and seek domains of existence of equilibria with non-vanishing overlapping segment. The parameter space includes the intrinsic curvatures of the rod and of the sleeve and also the initial length of the overlapping segment.

Keywords: nonlinear rods, sliding rods, stability, Hermite finite elements, non-material kinematic description, ALE

1 Introduction

Increasing practical demands and progress of novel problem specific simulation techniques promote the interest of researchers in modelling the dynamics and quasi-static behavior of axially moving structures, see review paper [1]. Moving transmission and transport belts, squealing brakes, band saws and elevator cables are examples of such structures. Systems featuring sliding rods represent a sub-class of axially moving structures, which is intensively investigated in the recent years both from the theoretical perspective as well as from the point of view of numerical simulations. The interesting problem of the elastica arm scale, in which a flexible rod is balanced in an inclined frictionless sleeve by configurational forces acting at the transition points was investigated theoretically and experimentally by Bosi et al. [2]; see also the analysis presented by O'Reilly [3]. The dynamic "sliding spaghetti" problem of a moving rod, partially inserted into a rigid sleeve was studied by Boyer et al. [4] as well es by Humer with co-authors [5–7]. When the motion within the sleeve is not kinematically prescribed but rather results from the overall dynamics of the flexible rod problem with moving boundaries, the configurational forces begin playing an important role as is visible in the surprising phenomenon of the "dancing rod", first demonstrated experimentally by Armanini et al. [8] and later analyzed numerically by Han and Bauchau in [9]. For the treatment of a spatial problem of rotation transmission by a rod with initial curvature in a curved channel we refer to [10].

The present contribution extends the spectrum of sliding rod problems by considering the case of a flexible sleeve with concentric tube robots [11] being possible practical motivation. In contrast to the latter reference, the study at hand is focused on the situation, when the relative sliding is not kinematically prescribed but rather results from the loading on the system and may lead to full ejection. The intrinsic curvatures (pre-curvatures) of the rod and of the sleeve are considered as load factors, resulting into deformation and relative sliding, which potentially ends up in full ejection. A problem specific non-material finite element scheme with C^1 inter-element continuity and an additional unknown in form of the configurational parameter is used to investigate the critical states in the space of parameters.

2 Problem statement

Schematically the problem under consideration is depicted in Fig. 1. Rod ① is partially inserted into a flexible sleeve ②, such that the overlapping region is bounded by transition points A and B. Because the sleeve will also be modelled as a rod, we simply speak about rod ① and rod ②, both being inextensible, having length ℓ and bending stiffness a (we assume the same bending stiffness to reduce the dimensionality of the parameter space). The compound rod will thus be having bending stiffness a in the first segment to the left of point A, where only rod ① is present and in the third segment to the right of point B, where only rod ② is present. The bending stiffness in the overlapping region (second segment) AB is $2a$. The length of the first segment

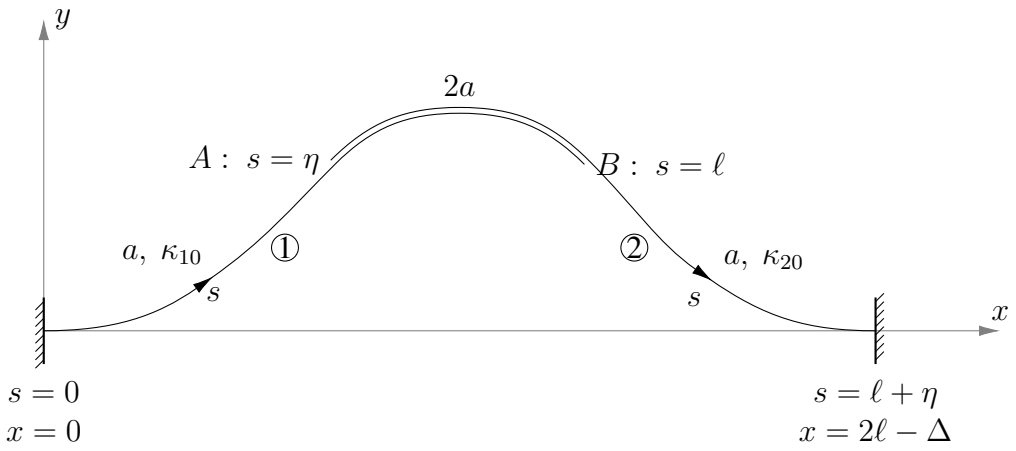

Figure 1: Flexible rod ① partially inserted in a flexible sleeve ② with transition points A and B; the small gap in the overlapping region AB is for visualization purpose only, here the geometries of both rods are identical

η is a configurational parameter and changes during the deformation of the structure because of the sliding of the rods. The length of the second segment is thus $\ell - \eta$, and the material length of the compound rod is $\ell + \eta$. The outer ends $s = 0$ and $s = \ell + \eta$ are either simply supported or clamped, but we kinematically prescribe the horizontal distance between them $2\ell - \Delta$ with Δ being the length of the overlapping region in the absence of deformation. The structure is loaded by intrinsic curvatures (pre-curvatures). The first rod has constant intrinsic curvature κ_{10}, such that being free from external actions it would take on the shape of an arc of a circle with the radius κ_{10}^{-1}. The intrinsic curvature of the second rod is κ_{20}. Changing these loading parameters, we obtain various deformed configurations with different values of η. The generalized force for this degree of freedom (which is frequently called configurational parameter) is the configurational force, which appears because of the jump of the curvature at the transition points. In the numerical procedure we will not need to explicitly consider this force because it is automatically taken into account when the total strain energy is minimized with respect to the deformed shape of the compound rod (nodal unknowns in the finite element model) and η.

For the sake of simplicity, we will consider a non-dimensional formulation with $\ell = 1$. Moreover, because the total strain energy is proportional to a, we also consider unit bending stiffness $a = 1$, which does not affect the deformed configurations. The condition of inextensibility is applied in the numerical procedure by penalizing the axial strain using tension stiffness $b = 10^4$, which is sufficiently high to result into practically converged solutions.

3 Strain energy

As mentioned earlier, for given parameters κ_{10}, κ_{20} and Δ the static configuration of the centerline of the compound rod provides minimum for its total strain energy U. We parametrize the position vector of a point on the centerline

$$\boldsymbol{x}(s) = x(s)\boldsymbol{e}_x + y(s)\boldsymbol{e}_y \tag{1}$$

as a function of the material arc-length coordinate s (which remains the arc-length during deformation because of inextensibility). This corresponds to the material (or Lagrangian) kinematic description, traditional in the structural mechanics. The total strain energy comprises three integrals over the segments:

$$\begin{aligned} U &= U_1 + U_2 + U_3, \\ U_1 &= \int_0^{\eta} \frac{1}{2}\left((\kappa-\kappa_{10})^2 + b\varepsilon^2\right)\,\mathrm{d}s, \\ U_2 &= \int_{\eta}^{1} \frac{1}{2}\left((\kappa-\kappa_{10})^2 + (\kappa-\kappa_{20})^2 + 2b\varepsilon^2\right)\,\mathrm{d}s, \\ U_3 &= \int_{1}^{1+\eta} \frac{1}{2}\left((\kappa-\kappa_{20})^2 + b\varepsilon^2\right)\,\mathrm{d}s. \end{aligned} \tag{2}$$

We denoted the geometric curvature of the inextensible rod and its negligibly small axial strain by

$$\begin{aligned} \kappa &= x'y'' - y'x'', \\ \varepsilon &= \frac{1}{2}\left(\boldsymbol{x}'\cdot\boldsymbol{x}' - 1\right) = \frac{1}{2}\left(x'^2 + y'^2 - 1\right). \end{aligned} \tag{3}$$

Prime in x' and y' stands for the derivative with respect to s. We seek static equilibria by minimizing the energy of the conservative system

$$U[\boldsymbol{x}(s), \eta] \to \min \tag{4}$$

with respect to the deformed centerline and the configurational parameter.

4 Non-material finite element model

Because η is not known in advance and the total length of the compound rod is changing, we cannot apply the standard finite element scheme with discretizing the material domain and assigning constant values of the material coordinate s to the nodes. Moreover, because of the jumps in the bending stiffness and in the curvature it would not be possible to simply scale the coordinate by a constant factor because it is clearly desirable to have a mesh, in which nodes are placed in the transition points A and B. This raises the need of transforming the formulation to the mixed Eulerian-Lagrangian kinematic description in the spirit of [12, 13].

We parametrize each of the three segments by a non-dimensional and non-material coordinate $\sigma \in [0,1]$ with a linear and solution dependent mapping to the material coordinate according to

$$\begin{aligned} &\text{segment 1:} \quad s = \sigma\eta, \\ &\text{segment 2:} \quad s = \eta + \sigma(1-\eta), \\ &\text{segment 3:} \quad s = 1 + \sigma\eta. \end{aligned} \tag{5}$$

Note that when η is changing, the mapping changes as well and the σ coordinate of a material particle $s = \text{const}$ will become different. The finite element approximation represents the position vector $\boldsymbol{x}$ as a function of σ in each segment. The requirement of C^1 inter-element continuity (no jumps in $\boldsymbol{x}'(s)$) makes the choice of cubic Hermite shape functions natural, see [10, 14] for a general discussion of C^1 continuous approximation of the deformed geometry in modelling geometrically nonlinear rods. We divide each segment into n elements with length $1/n$ in terms of σ and introduce a local element coordinate $\xi \in [-1,1]$. An element number $i = 1 \ldots n$ is bounded by nodes $i-1$, i with degrees of freedom $\boldsymbol{x}_i$ and $(\partial_\xi \boldsymbol{x})_i$, that is 4 scalar degrees of freedom per node. The deformed shape of the element is now parametrized as

$$\boldsymbol{x} = S_1(\xi)\boldsymbol{x}_{i-1} + S_2(\xi)(\partial_\xi \boldsymbol{x})_{i-1} + S_3(\xi)\boldsymbol{x}_i + S_4(\xi)(\partial_\xi \boldsymbol{x})_i \tag{6}$$

with cubic shape functions

$$[S_1, S_2, S_3, S_4] = \frac{1}{4}\left[2 - 3\xi + \xi^3, (\xi-1)^2(\xi+1), 2 + 3\xi - \xi^3, (\xi-1)(\xi+1)^2\right] \tag{7}$$

fulfilling the conditions

$$\begin{bmatrix} S_1(-1) & \partial_\xi S_1(-1) & S_1(1) & \partial_\xi S_1(1) \\ S_2(-1) & \partial_\xi S_2(-1) & S_2(1) & \partial_\xi S_2(1) \\ S_3(-1) & \partial_\xi S_3(-1) & S_3(1) & \partial_\xi S_3(1) \\ S_4(-1) & \partial_\xi S_4(-1) & S_4(1) & \partial_\xi S_4(1) \end{bmatrix} = \begin{bmatrix} 1 & 0 & 0 & 0 \\ 0 & 1 & 0 & 0 \\ 0 & 0 & 1 & 0 \\ 0 & 0 & 0 & 1 \end{bmatrix}. \tag{8}$$

This choice of shape functions guarantees the continuity of $\boldsymbol{x}$ and $\partial_\xi \boldsymbol{x}$ across the boundaries of the finite elements, which means the continuity of $\boldsymbol{x}'$ because of the proportionality of the derivatives. However, this simple formulation results into jumping $\boldsymbol{x}'$ across the boundaries of the segments in points A and B, in which $\partial_s \sigma$ is discontinuous, which needs to be repaired by a simple extension of the finite element approximation Eq. (6). It retains its look in the segments 1 and 3, and in the overlapping segment 2 we replace it by

$$\boldsymbol{x} = S_1(\xi)\boldsymbol{x}_{i-1} + S_2(\xi)\left(\frac{1}{\eta} - 1\right)(\partial_\xi \boldsymbol{x})_{i-1} + S_3(\xi)\boldsymbol{x}_i + S_4(\xi)\left(\frac{1}{\eta} - 1\right)(\partial_\xi \boldsymbol{x})_i. \tag{9}$$

This solution-dependent scaling of the nodal derivatives in one of the segments exactly compensates the jumps in $\partial_s \sigma$, thus providing continuity of $\boldsymbol{x}'$ in points A and B

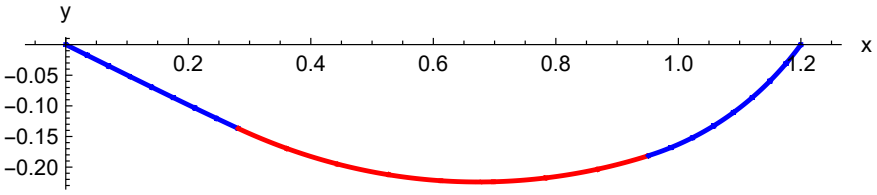

Figure 2: Deformed shape, simply supported ends, $\kappa_{10} = 0$, $\kappa_{20} = 1.9$, $\Delta = 0.8$; segments 1 and 3 are depicted blue, and segment 2 (overlapping region) is plotted red

when the degrees of freedom of the node n in the segments 1 and 2 are respectively identified with the degrees of freedom of the node 0 in segments 2 and 3. Counting η among the overall set of degrees of freedom of the model, we thus obtain a nonlinear finite element approximation – which can, however, easily be treated using computer algebra software[1]. We integrate the energy over each finite element using Gaussian rule with 3 quadrature points and assemble the total expression for U as a function of all nodal degrees of freedom and η, which we then minimize using the respective routine. The boundary conditions impose additional constraints:

$$\begin{aligned} &\text{segment 1:} \quad x_0 = 0,\ y_0 = 0,\ \text{if clamping: } (\partial_\xi y)_0 = 0, \\ &\text{segment 3:} \quad x_n = 2 - \Delta,\ y_n = 0,\ \text{if clamping: } (\partial_\xi y)_n = 0. \end{aligned} \tag{10}$$

5 Simulation results: deformed configurations

Choosing specific values of κ_{10}, κ_{20}, Δ and type of boundary conditions, we directly minimize U using the straight configuration with $\eta = 1 - \Delta$ as initial approximation. Practically converged solutions were obtained with $n = 8$ finite elements in each segment, we used this discretization for obtaining the results in the following. At first we study the deformed shapes of the structure with simply supported end points and relatively high initial injection $\Delta = 0.8$, which allows for larger deformations until the stability loss and full ejection. The situation, where just one of the rods has intrinsic curvature is presented in Fig. 2; the red part of the line corresponds to the overlapping region. The configuration is slightly unsymmetric and the "injection depth" is relatively high for the chosen value $\kappa_{20} = 1.9$ – although we will soon see that this state is close to the stability boundary, and slight growth of the curvature would result into complete ejection. Next we consider the case of equal natural curvatures in Fig. 3. Much higher deformation level can be reached now such that the overlapping region shrinks with no loss of stability. A solution with different signs of initial curvatures is presented in Fig. 4. At $\kappa_{10} = -\kappa_{20}$ the linear terms with κ vanish in the integral for U_2 in Eq. (2), which makes the compound rod free from natural curvature in the overlapping region. Still there is curvature in the deformed shape of the straight line because

[1]We implemented the simulation using Wolfram Mathematica, see `https://wolfram.com/mathematica`.

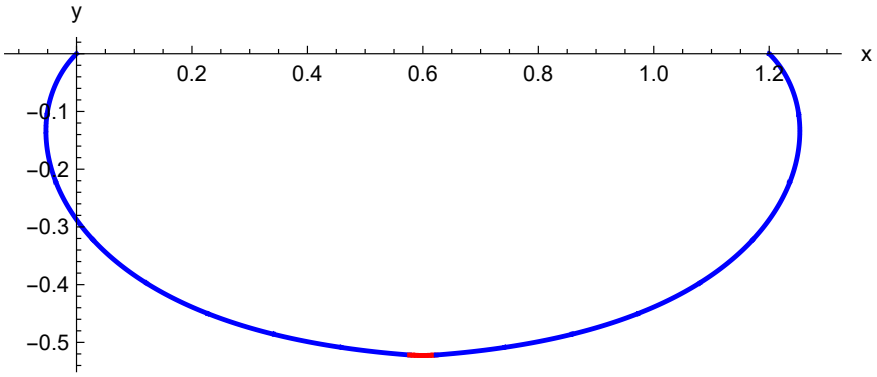

Figure 3: Deformed shape, simply supported ends, $\kappa_{10} = 6$, $\kappa_{20} = 6$, $\Delta = 0.8$

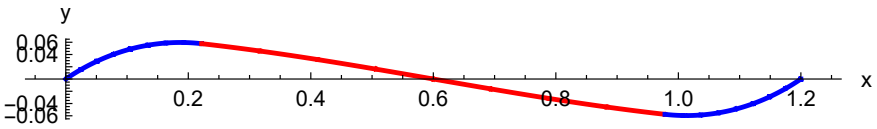

Figure 4: Deformed shape, simply supported ends, $\kappa_{10} = -2.6$, $\kappa_{20} = 2.6$, $\Delta = 0.8$

of the horizontal reaction forces in the supports. Fig. 5 and Fig. 6 show that much higher intrinsic curvatures are possible when the end points of the rods are clamped.

6 Simulation results: boundaries of existence of solutions with partial injection

For both types of the boundary conditions and three different values of initial injection $\Delta = 0.4, 0.6, 0.8$ we investigated the shape of the boundary of the domain in the parameter space $(\kappa_{10}, \kappa_{20})$, in which the solutions with partial rod contact and non-vanishing overlapping region exist. For this sake we performed the simulation for $\kappa_{10} = \kappa_0 \cos\theta$ and $\kappa_{20} = \kappa_0 \sin\theta$, increasing κ_0 in small steps as long as the numerical minimization of U produced physically meaningful solution with $\eta < 1$. Solution from the previous step was used as starting approximation for the subsequent minimization to follow a continuous equilibrium path, and the incrementation steps were automatically reduced to obtain critical values with desired accuracy. Additionally, we took care that η would steadily grow from step to step to avoid jumps to complicated equilibria with self-intersections, which were otherwise eventually observed. Changing θ in small steps from 0 to π, we collected the critical values $\kappa_{0*}(\theta)$, thus forming the stability boundary in polar coordinates.

For the simply supported ends the results are demonstrated in Fig. 7. The stability zone is getting larger with growing Δ. For $\Delta = 0.4$ and $\Delta = 0.6$ the highest overall level of initial curvatures is reached when $\theta = 3\pi/4$ and $\kappa_{10} = -\kappa_{20}$. However, from the lower part of Fig. 7 we see that much higher curvature level is possible at $\Delta = 0.8$ in the vicinity of $\theta = \pi/4$, where $\kappa_{10} \approx \kappa_{20}$, that is when the deformed

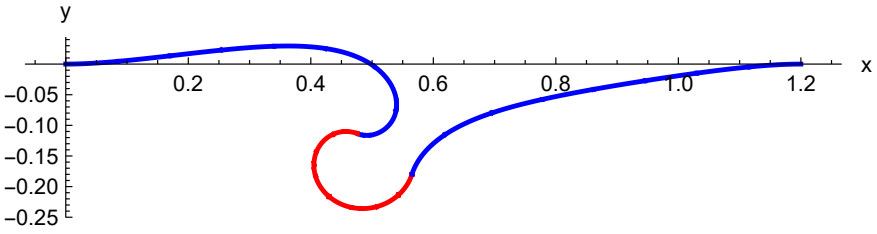

Figure 5: Deformed shape, clamped end points, $\kappa_{10} = 40$, $\kappa_{20} = 60$, $\Delta = 0.8$

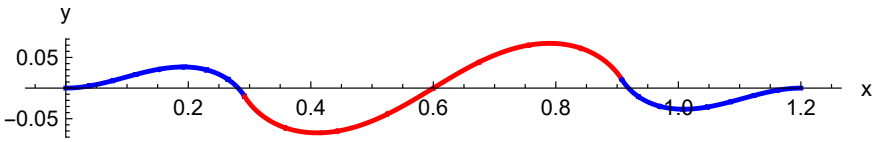

Figure 6: Deformed shape, clamped end points, $\kappa_{10} = -29$, $\kappa_{20} = 29$, $\Delta = 0.8$

shapes are nearly symmetric. This interesting effect requires further investigation. The open question is whether further stable solution branches could be detected if we continuously move away from the obtained stable solutions downwards or to the left, which was not covered by the current simple investigation.

The stability boundaries for clamped ends are depicted in Fig. 8. Interestingly, much higher loading is possible in the antisymmetric range $\kappa_{10} \approx -\kappa_{20}$ when $\Delta = 0.4$, and for positive intrinsic curvatures the domains of stability for all three values of the initial injection are quite similar.

7 Concluding remarks

For the problem of frictionless contact of an elastic rod and a flexible sleeve we presented a novel simulation technique, which makes use of a non-material finite element approximation: the nodes of the finite element mesh are not bound to material particles, the latter may thus travel from element to element when the structure is deforming. Depending on the natural curvatures of the rod and the sleeve, on the initial injection length and the type of the boundary conditions various deformed shapes of the compound structure in equilibrium are observed. Stability loss and complete ejection is possible when the natural curvatures exceed critical values. A numerical investigation of the stability zones in the parameter space provides non-trivial results and raises open questions concerning the existence of distant branches of the equilibrium path.

References

[1] J. Scheidl, Y. Vetyukov "Review and perspectives in applied mechanics of axially moving flexible structures", Acta Mechanica, 234(4), 1331-1364, 2023.

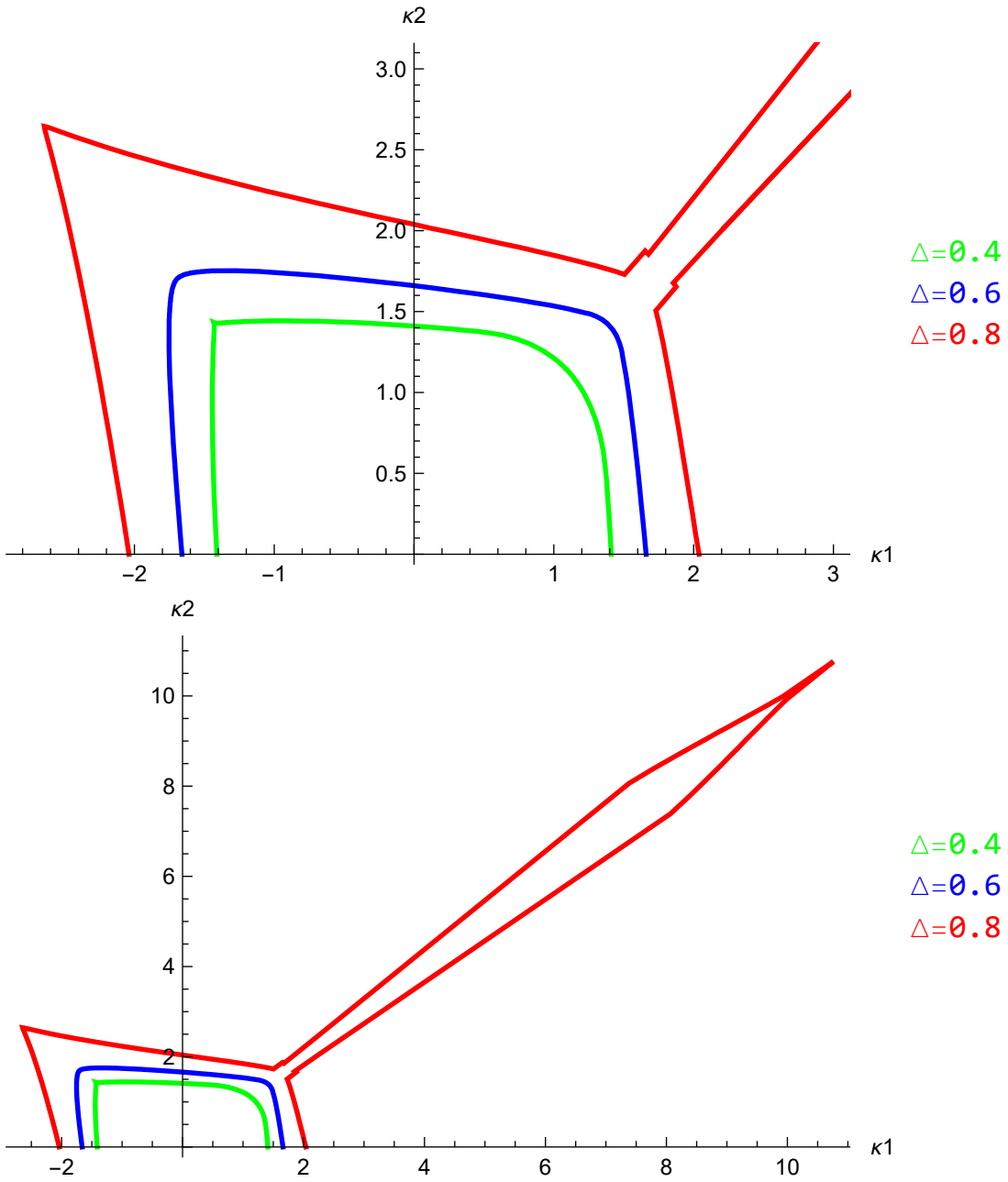

Figure 7: Boundaries of the zone of existence of partially injected solution in parameter space in dependence on Δ for simply supported end points; zoomed image and full picture

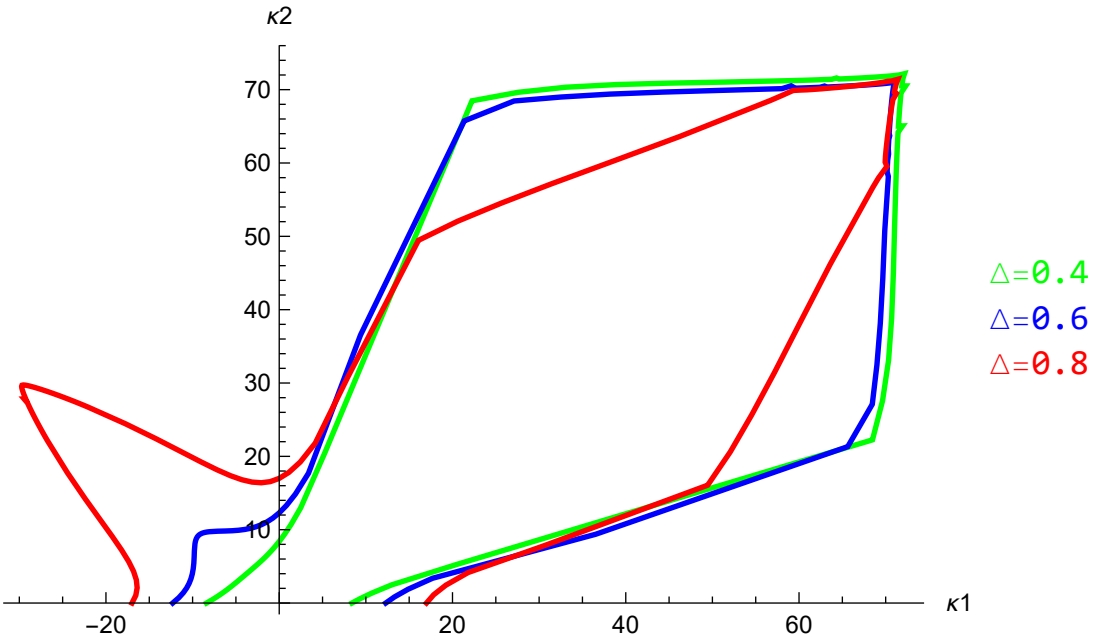

Figure 8: Boundaries of the zone of existence of partially injected solution in parameter space in dependence on Δ for clamped end points

[2] F. Bosi, D. Misseroni, F. Dal Corso, D. Bigoni, "An elastica arm scale", Proceedings of the Royal Society A, 470, 20140232, 2014.

[3] O.M. O'Reilly, Modeling nonlinear problems in the mechanics of strings and rods, Cham: Springer International Publishing, Switzerland, 2017.

[4] F. Boyer, V. Lebastard, F. Candelier, F. Renda, "Extended Hamilton's principle applied to geometrically exact Kirchhoff sliding rods", Journal of Sound and Vibration, 516:116511, 2022.

[5] A. Humer, "Dynamic modeling of beams with non-material, deformation-dependent boundary conditions", Journal of Sound and Vibration, 332(3), 622–641, 2013.

[6] I. Steinbrecher, A. Humer, L. Vu-Quoc, "On the numerical modeling of sliding beams: a comparison of different approaches", Journal of Sound and Vibration, 408, 270–290, 2017.

[7] A. Humer, I. Steinbrecher, L. Vu-Quoc, "General sliding-beam formulation: a non-material description for analysis of sliding structures and axially moving beams", Journal of Sound and Vibration, 480, 115341, 2020.

[8] C. Armanini, F. Dal Corso, D. Misseroni, D. Bigoni, "Configurational forces and nonlinear structural dynamics", Journal of the Mechanics and Physics of Solids, 130, 82-100, 2019.

[9] S. Han, O.A. Bauchau, "Configurational forces in variable-length beams for flexible multibody dynamics", Multibody System Dynamics, 58(3), 275-298, 2023.

[10] Y. Vetyukov, E. Oborin, "Snap-through instability during transmission of rotation by a flexible shaft with initial curvature", International Journal of Non-

Linear Mechanics, 154, 104431, 2023.
[11] F. Renda, C. Messer, C. Rucker, F. Boyer, "A sliding-rod variable-strain model for concentric tube robots", IEEE Robotics and Automation Letters, 6(2), 3451-3458, 2021.
[12] Y. Vetyukov, "Non-material finite element modelling of large vibrations of axially moving strings and beams", Journal of Sound and Vibration, 414, 299-317, 2018.
[13] Y. Vetyukov, E. Oborin, J. Scheidl, M. Krommer, C. Schmidrathner. "Flexible belt hanging on two pulleys: contact problem at non-material kinematic description", International Journal of Solids and Structures, 168, 183-193, 2019.
[14] Y. Vetyukov, "Hybrid asymptotic-direct approach to the problem of finite vibrations of a curved layered strip", Acta Mechanica, 223(2), 371-385, 2012.